

Reinforcement Learning for Freeway Lane-Change Regulation via Connected Vehicles

Ke Sun, and Huan Yu, *Member, IEEE*

arXiv:2412.04341v2 [eess.SY] 6 Dec 2024

Abstract—Lane change decision-making is a complex task due to intricate vehicle-vehicle and vehicle-infrastructure interactions. Existing algorithms for lane-change control often depend on vehicles with a certain level of autonomy (e.g., autonomous or connected autonomous vehicles). To address the challenges posed by low penetration rates of autonomous vehicles and the high costs of precise data collection, this study proposes a dynamic lane change regulation design based on multi-agent reinforcement learning (MARL) to enhance freeway traffic efficiency. The proposed framework leverages multi-lane macroscopic traffic models that describe spatial-temporal dynamics of the density and speed for each lane. Lateral traffic flow between adjacent lanes, resulting from aggregated lane-changing behaviors, is modeled as source terms exchanged between the partial differential equations (PDEs). We propose a lane change regulation strategy using MARL, where one agent is placed at each discretized lane grid. The state of each agent is represented by aggregated vehicle attributes within its grid, generated from the SUMO microscopic simulation environment. The agent’s actions are lane-change regulations for vehicles in its grid. Specifically, lane-change regulation signals (e.g., "left change allowed" or "right change disallowed") are computed at a centralized traffic management center and then broadcast to connected vehicles in the corresponding lane grids. Compared to vehicle-level maneuver control, this approach achieves a higher regulation rate by leveraging vehicle connectivity while introducing no critical safety concerns, and accommodating varying levels of connectivity and autonomy within the traffic system. The proposed model is simulated and evaluated in varied traffic scenarios and demand conditions. Experimental results demonstrate that the method improves overall traffic efficiency with minimal additional energy consumption while maintaining driving safety.

Index Terms—Multi-agent reinforcement learning, traffic flow, lane change regulation, macroscopic traffic model.

I. INTRODUCTION

Freeway traffic control has relied on infrastructure-based measures such as speed limits and ramp traffic lights. Recently, there has been a growing focus on leveraging connected automated vehicles (CAVs) for traffic flow improvement. The cruising behaviors of the CAVs are controlled to enhance traffic stability [1]–[4], safety [5]–[7], energy consumption [8]–[10], and efficiency [3], [11]–[13]. While significant advancements have been achieved in longitudinal vehicle and platoon control, lateral control—particularly in lane change control—remains a challenging task due to the complexity of optimization in a higher-dimensional solution space.

Ke Sun and Huan Yu are with the Hong Kong University of Science and Technology (Guangzhou), Thrust of Intelligent Transportation, Guangzhou, Guangdong, China. (kes@hkust-gz.edu.cn, huanyu@ust.hk). This work was supported by the National Natural Science Foundation of China No.62203131 and Guangzhou Municipal Education Bureau University Project 2024312102.

Huan Yu is the corresponding author. Email: *huanyu@ust.hk*

Many studies focus on ramp-merging areas in freeway traffic control, where mandatory lane changes of ramp-merging vehicles can cause substantial disturbances to mainline traffic. Traditionally, macroscopic approaches such as ramp metering have been employed to control the inflow from on-ramps. Classical methods include the feedback control strategy ALINEA [14] and its extensions [15]–[17]. More recently, Deep Reinforcement Learning (DRL)-based approaches have been explored to achieve superior performance under model uncertainty and incomplete information [18]–[21]. With advances in connectivity and autonomy technologies, CAVs offer an opportunity to control individual vehicles in ramp-merging areas instead of relying solely on aggregated control. A classical method is to map the merging problem to a platoon control framework using virtual mapping [22]–[24]. Beyond this mapping framework, optimization-based methods have been proposed to search for optimal solutions [25]–[27]. DRL-based methods have also been introduced [28], [29].

Another critical challenge involves managing lane changes on freeways to improve traffic efficiency, which is the primary focus of our work. Studies such as [30], [31] demonstrate that lane changes significantly impact traffic safety and efficiency. Further research shows that CAVs can enhance these metrics in traffic congestion, particularly with high CAV penetration rates [32], [33]. At the macroscopic level, an implicit strategy for managing lane changes is the implementation of restricted-use lanes, such as High Occupancy Vehicle (HOV) lanes [34], [35]. To optimize individual lane change decisions and trajectories, researchers have developed collaborative driving strategies. For example, game-theory-based methods, such as the Nash bargaining approach in [36], aim to optimize traffic flow. Optimization-based methods [37], [38] seek to mitigate congestion near conflict areas by coordinating CAV lane change decisions. Additionally, Multi-Agent Reinforcement Learning (MARL) methods have been proposed to achieve robust generalization performance [39], [40].

However, existing DRL models for lane change control face two significant challenges. First, given the expected low penetration of CAVs in the near future, performance under varying penetration rates must be carefully evaluated. Experimental findings in [3] reveal that while CAVs can enhance traffic stability, substantial improvements are primarily observed at higher penetration rates. Second, the accurate collection of traffic state information, particularly in large-scale environments, is often prohibitively expensive or even infeasible. Many existing approaches assume robust vehicle-to-vehicle or vehicle-to-infrastructure communication. However, as noted in [41], challenges such as communication latency, limited data bandwidth, and privacy concerns can impede the effectiveness

of centralized training schemes.

To address these deficiencies, we propose a centralized traffic flow control strategy within a multi-agent reinforcement learning (MARL) framework. This strategy regulates lane-changing behaviors of connected vehicles (CVs) at the macroscopic level to enhance the overall efficiency of mixed freeway traffic. Inspired by infrastructure-based control methods such as ramp metering and restricted-use lanes for freeway management, our model employs an infrastructure-based regulation framework that operates at the decision level. Regulation signals—either permitting or prohibiting maneuvers—are dispatched through a traffic management center to CVs. The minimal regulation units in our model are spatially discretized cells of the macroscopic PDE model, referred to as lane grids, rather than individual vehicles as targeted by prior MARL-based lane change control approaches.

This design provides two significant advantages in overcoming the aforementioned challenges. First, our regulation model requires only connectivity functionalities in vehicles, avoiding reliance on high levels of autonomy. Consequently, it regulates a wide range of vehicle types, including human-driven vehicles (HVs), by equipping them with vehicle-to-infrastructure communication technologies. Our proposed approach enables broader compatibility and achieves a higher regulation rate compared to CAV-specific control methods. Second, the macroscopic representation substantially reduces data transmission requirements and eliminates the need for precise vehicle positioning, thereby enhancing scalability and practicality in real-world applications.

This paper theoretically addresses in-domain distributed control of PDE systems using a robust MARL framework. Two closely related works are [18], [19], which propose scalable ramp metering control via MARL applied to the traffic PDE models. Several studies have also demonstrated the successful application of MARL to PDE dynamics in diverse domains, including fluid flow control, drag reduction, and turbulence modeling [42]–[44], and [45] further provides a theoretical foundation for distributed PDE control using MARL.

The main contributions of this work are summarized as follows:

- 1) We propose a novel fine-resolution, lane-grid-based lane-change regulation approach for freeway traffic control. The infrastructure-based framework is leveraged to enhance traffic efficiency by regulating lane-change maneuvers at a macroscopic level via a centralized control strategy.
- 2) In contrast to traditional MARL-based vehicle control methods, the proposed traffic flow control strategy simplifies communication requirements and reduces reliance on precise vehicle positioning, enabling efficient and scalable implementation in large-scale traffic systems.
- 3) We establish a hierarchical RL framework by utilizing a microscopic simulator to generate microscopic vehicle trajectories and adopting the multi-lane macroscopic traffic PDEs to compute aggregated lane-change decisions for CVs, thereby improving freeway traffic performance.

To the best of our knowledge, this is the first attempt to employ a fine-resolution lane-change regulation model for freeway lane management on CVs. Positioned between infrastructure-level control and direct lane-change maneuver control, our regulation model minimizes information collection burdens while managing lane changes at a macroscopic level without introducing additional safety risks.

This paper is organized as follows. Section II details the modeling of our control problem using PDEs and derives the distributed regulation framework using multi-agent reinforcement learning. Section III-A describes the setup of our experimental environments in the SUMO microscopic simulator. Section IV presents extensive numerical results demonstrating the performance of the proposed model. Finally, Section V concludes the paper.

II. LANE CHANGE REGULATION MODEL

In this section, we first describe the freeway traffic dynamics with lane-change using a generic multi-lane macroscopic traffic flow model, and then propose a multi-agent reinforcement learning control formulation to address this problem.

A. Multi-lane Macroscopic Traffic Models

The simplest first-order model for general one-lane traffic is the Lighthill-Whitham-Richards (LWR) model,

$$\frac{\partial \rho}{\partial t} + \frac{\partial f}{\partial x} = 0 \quad (1)$$

where ρ represents the vehicle density, f denotes the traffic flow rate, t is time, and x is the spatial position [46]. The flow f is modeled as a function of density: $f = Q(\rho)$ using a fundamental diagram. While this model captures traffic shockwaves, it cannot represent speed oscillations such as stop-and-go waves due to its adoption of equilibrium vehicle speed and density relation. Second-order models, such as the Aw-Rascle-Zhang (ARZ) model [47], [48], introduce an additional equation for vehicle velocity. These models are better suited for capturing traffic waves, acceleration, and deceleration effects in traffic flow.

To extend single-lane macroscopic models to multi-lane traffic flow, the lateral traffic flow between lanes, as a result of accumulated lane-change trajectories of individual vehicles, need to be modeled explicitly.

We consider a highway of length L with $m \in \mathbb{N}$ lanes, and a traffic flow over a time period T . A source-sink term representing mass exchange with neighboring lanes appears on the right-hand side of the conservation law in Eq. (1) for each lane α :

$$\frac{\partial \rho_\alpha}{\partial t} + \frac{\partial f_\alpha}{\partial x} = \text{Gain}_\alpha - \text{Loss}_\alpha \quad (2)$$

We assume vehicles in the flow are homogeneous, meaning that all vehicles share the same lane change criterion and action time, τ_{lc} . Let $p_{\alpha_1, \alpha_2}(x_i)$ represent the fraction of vehicles in the i -th grid of lane α_1 that intend to change to lane α_2 (either $\alpha_1 - 1$ or $\alpha_1 + 1$). The transition rates, $1/T^{\text{left}}$ and $1/T^{\text{right}}$ are given by:

$$\begin{aligned} \frac{1}{T_{\alpha-1}^{\text{left}}}(x_i) &= \frac{p_{\alpha,\alpha-1}(x_i)}{\tau_{lc}} \\ \frac{1}{T_{\alpha+1}^{\text{right}}}(x_i) &= \frac{p_{\alpha,\alpha+1}(x_i)}{\tau_{lc}} \end{aligned} \quad (3)$$

In [49], [50], transition rates are modeled and calibrated based on vehicle interactions and traffic regulation criteria. In an uncontrolled system without lane-change regulation, the evolution of the conservation law is expressed as follows:

$$\frac{\partial \rho_\alpha}{\partial t} + \frac{\partial f_\alpha}{\partial x} = \left(\frac{\rho_{\alpha-1}}{T_{\alpha-1}^{\text{left}}} + \frac{\rho_{\alpha+1}}{T_{\alpha+1}^{\text{right}}} \right) - \left(\frac{\rho_\alpha}{T_\alpha^{\text{right}}} + \frac{\rho_\alpha}{T_\alpha^{\text{left}}} \right) \quad (4)$$

The evolution of the conservation law in a fully controllable traffic system is expressed as:

$$\begin{aligned} \frac{\partial \rho_\alpha}{\partial t} + \frac{\partial f_\alpha}{\partial x} &= \left(\frac{\rho_{\alpha-1}}{T_{\alpha-1}^{\text{left}}} a_{\alpha-1}^{\text{left}} + \frac{\rho_{\alpha+1}}{T_{\alpha+1}^{\text{right}}} a_{\alpha+1}^{\text{right}} \right) \\ &\quad - \left(\frac{\rho_\alpha}{T_\alpha^{\text{left}}} a_\alpha^{\text{left}} + \frac{\rho_\alpha}{T_\alpha^{\text{right}}} a_\alpha^{\text{right}} \right) \end{aligned} \quad (5)$$

where the action $a_\alpha^{\text{left}}, a_\alpha^{\text{right}} \in \mathbb{R}$ regulates the magnitude of vehicle mass exchange caused by lane changes between adjacent lane grids in the respective directions (left or right).

In addition to the evolution of traffic density ρ_α , the evolution of velocity v_α in our system must also be considered. Several studies [51], [52] propose multi-lane second-order PDE models that describe velocity and density separately. The general form of the momentum equation governing the evolution of velocity is given as:

$$\begin{aligned} \frac{\partial(\rho_\alpha v_\alpha)}{\partial t} + \frac{\partial(\rho_\alpha v_\alpha^2)}{\partial x} &= -\frac{\partial p(\rho_\alpha)}{\partial x} + \rho_\alpha R(\rho_\alpha, v_\alpha) + S(\rho, v) \\ S(\rho, v) &= \left(\frac{\rho_{\alpha-1} v_{\alpha-1}}{T_{\alpha-1}^{\text{left}}} a_{\alpha-1}^{\text{left}} + \frac{\rho_{\alpha+1} v_{\alpha+1}}{T_{\alpha+1}^{\text{right}}} a_{\alpha+1}^{\text{right}} \right) \\ &\quad - \left(\frac{\rho_\alpha v_\alpha}{T_\alpha^{\text{left}}} a_\alpha^{\text{left}} + \frac{\rho_\alpha v_\alpha}{T_\alpha^{\text{right}}} a_\alpha^{\text{right}} \right) \end{aligned} \quad (6)$$

where the relaxation term $R(\rho_\alpha, v_\alpha)$ describes how vehicles approach their steady-state speed corresponding to the local density, and the pressure term $p(\rho_\alpha)$ captures the response of the local vehicle ensemble to density gradients [46]. The source term $S(\rho, v)$ quantifies the momentum exchange due to lane changes, consistent with the mass exchange in Eq. (5).

Eq. (6) accurately represents macroscopic dynamics in our simulation environment, where vehicle dynamics follow microscopic physical models. Several works [53], [54] investigate the connection between specific microscopic and macroscopic models for multi-lane traffic dynamics.

Combining Eqs. (5) and (6), we represent the second-order traffic PDE model in vector form as:

$$\frac{\partial y_\alpha}{\partial t} + A(y_\alpha) \frac{\partial y_\alpha}{\partial x} = S(y_{\alpha-1}, y_\alpha, y_{\alpha+1}, a_{\alpha-1}, a_\alpha, a_{\alpha+1}) \quad (7)$$

where

$$y_\alpha = \begin{pmatrix} \rho_\alpha \\ v_\alpha \end{pmatrix} \quad (8)$$

Here, $A(y_\alpha)$ governs the characteristic speeds of the system, and $S(y_{\alpha-1}, y_\alpha, y_{\alpha+1}, a_{\alpha-1}, a_\alpha, a_{\alpha+1})$ denotes mass exchange and momentum exchange due to lane changes. Various second-order PDE traffic models are discussed in [48], with different designs for A and S .

When considering the dynamics of all lanes, the PDE model becomes:

$$\frac{\partial y}{\partial t} + A(y) \frac{\partial y}{\partial x} = S(y, a) \quad (9)$$

where state $y = (\rho_1, v_1, \dots, \rho_m, v_m)^T$ and action $a = (a_1^{\text{left}}, a_1^{\text{right}}, \dots, a_m^{\text{left}}, a_m^{\text{right}})^T$. We can rewrite Eq. (9) using a partial differential operator:

$$\frac{\partial y}{\partial t} = \mathcal{N}(y, a) = -A(y) \frac{\partial y}{\partial x} + S(y, a) \quad (10)$$

B. Grid-based Lane Change Regulation Strategies

We discretize the system both temporally and spatially. The spatial domain $[0, L]$ is divided into equally spaced intervals, each with grid length Δx , such that a lane is divided into $N_x = L/\Delta x$ grids. The time domain $[0, T]$ is partitioned with time-steps $\Delta T = t_q - t_{q-1}$, where $q = 1, \dots, N_T$.

Let there be M vehicles at time t_k . The longitudinal position of vehicle m in lane α^m , denoted by $x_{\alpha^m}^m(t_k)$, and its velocity $v_{\alpha^m}^m(t_k)$, are discrete values. To incorporate the microscopic data into a PDE model, we need to compute the macroscopic traffic state for each spatial grid. [55] employs a kernel density estimation (KDE) method to estimate density, velocity, and flow functions for the PDE model. Our approach adopts a simpler version of KDE, where each grid is represented by an averaged quantity, rather than requiring detailed positional data. This simplification reduces the need for precise vehicle positioning.

Specifically, the density at the i -th grid in lane α is computed by counting the number of vehicles within the grid centered at x_i :

$$\begin{aligned} \rho_{\alpha_i} &= \frac{N_{\alpha_i}}{\Delta x} \\ N_{\alpha_i} &= \sum_{m=1}^M \mathbf{1}_{[x_i - \frac{\Delta x}{2}, x_i + \frac{\Delta x}{2}], \alpha^m = \alpha}(x_{\alpha^m}^m) \end{aligned} \quad (11)$$

The velocity in the same grid is estimated by averaging the velocities of all vehicles within the grid:

$$v_{\alpha_i} = \frac{1}{N_{\alpha_i}} \sum_{m:x^m \in [x_i - \frac{\Delta x}{2}, x_i + \frac{\Delta x}{2}], \alpha^m = \alpha} (v_{\alpha^m}^m) \quad (12)$$

The flow is then calculated by multiplying the estimated density and velocity:

$$f_{\alpha_i} = \rho_{\alpha_i} \cdot v_{\alpha_i} \quad (13)$$

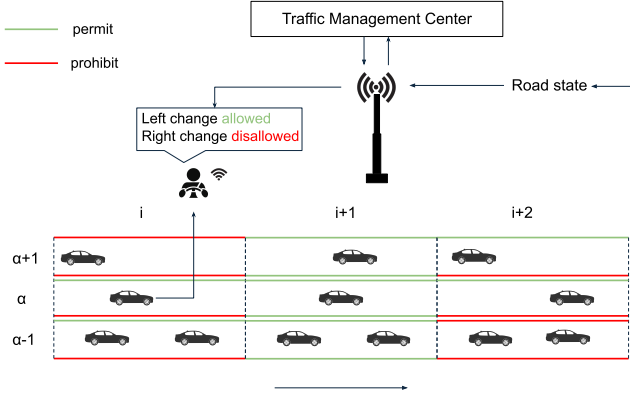


Fig. 1. Model demonstration of lane change regulation signals broadcast to drivers via traffic management center.

Our model operates by enabling or disabling source terms in Eq. (5) and (6) based on the regulation commands. Within our system, we assume the presence of two types of vehicles: HVs, which execute lane changes without intervention from the regulation model, and CVs, which are HVs equipped with connectivity technologies that adhere strictly to regulation signals. Notably, both CVs and HVs follow the same microscopic dynamic models. Unlike an uncontrolled system, where lane change requests are automatically permitted, our model enables selective control by either permitting or prohibiting lane changes of CVs from grid α_i to its neighboring grid in an adjacent lane. Fig. 1 illustrates how our model functions in a real-world scenario by broadcasting lane change regulations to vehicles through road infrastructure.

The action for any grid α_i at time t_k is represented as a two-dimensional vector:

$$a_{\alpha_i}(t_k) = (a_{\alpha_i}^{\text{left}}(t_k), a_{\alpha_i}^{\text{right}}(t_k)) \in \{0, 1\}^2 \quad (14)$$

where each component indicates whether lane change requests towards a specific direction from vehicles in grid α_i at time t_k are permitted. In Eq. (5) and (6), if the action blocks a lane change path, any request for that path is disallowed, effectively preventing the corresponding gain or loss term by multiplying it with the action value 0. Otherwise, the source term behaves as in the uncontrolled case.

In the context of reinforcement learning, the discretized transition function expressed using the partial differential operator in Eq. (10) for each grid column is:

$$\begin{aligned} y_{x=x_i}(t_{k+1}) &= f_{x_i}(y(t_k), a(t_k)) \\ &= y_{x=x_i}(t_k) + \int_{t_k}^{t_{k+1}} \mathcal{N}(y(\tau), a(t_k)) d\tau |_{x=x_i} \end{aligned} \quad (15)$$

where the action $a_{x_i}(t_k)$ is held constant during the time interval (zero-order hold).

In the hyperbolic PDE model, wave propagation occurs at finite speeds, so the evolution of a grid over a short

time depends only on a localized region of the state. Let $\mathcal{I}_{\Delta t}(x_i) \subset \{x_1, \dots, x_{N_x}\}$ represent the local region around x_i within the maximum wave propagation distance (Δt times the maximum wave speed). This region is determined by the time step Δt and the PDE model's properties, independent of the specific location x_i . The transition function is given by:

$$y_{x=x_i}(t_{k+1}) = \tilde{f}_{x_i}(y_{\mathcal{I}_{\Delta t}(x_i)}(t_k), a_{\mathcal{I}_{\Delta t}(x_i)}(t_k)) \quad (16)$$

The dynamics in Eq. (10) exhibit spatial translation invariance, meaning the system's behavior does not depend on specific spatial locations when border effects are negligible and the grid size L is sufficiently large. This property ensures identical local environments for all grid columns, i.e., $\tilde{f} = \tilde{f}_{x_1} = \dots = \tilde{f}_{x_{N_x}}$, enabling parameter sharing across grid columns.

Two further approximations are made in the training algorithm design:

- 1) We assume identical geometric characteristics, speed limits, and lane discipline across all lanes in each simulated environment. Neglecting border effects (e.g., where border lanes have only one adjacent lane), spatial translation invariance extends to all grids. Consequently, we assign one agent to each grid and train a model with shared parameters across the entire grid system.
- 2) The dynamics during safety-critical events may evolve with a spatially inhomogeneous partial differential operator, deviating from Eq. (10). However, since these anomalies are confined to a small fraction of the overall space-time domain, we neglect them during training and evaluation.

C. Multi-agent Reinforcement Learning

We address the control problem using multi-agent reinforcement learning. The overall architecture of the proposed lane change regulation system is illustrated in Fig. 2. Each grid has an agent, and all agents share network parameters. The target system is formulated as a Partially Observable Markov Decision Process (POMDP). Formally, a POMDP can be represented as a 6-tuple $(\mathcal{S}, \mathcal{A}, \mathcal{P}, \mathcal{R}, \Omega, \mathcal{O})$, where \mathcal{S} denotes the state space, Ω represents the observation space, \mathcal{A} is the action space, $\mathcal{P} : \mathcal{S} \times \mathcal{A} \rightarrow \mathcal{S}$ describes the state transition distribution, \mathcal{O} is the probabilistic observation model, and \mathcal{R} is the reward function.

1) *State space*: The entire state space of the highway is defined as $\mathcal{S} = \times_{\alpha \in \{1, \dots, m\}, i \in \{1, \dots, N_x\}} S_{\alpha_i}$, where S_{α_i} represents the state of the grid α_i . Features encoded in each state include:

- ρ : the total vehicle density within the grid.
- ρ_c : the CV density within the grid, where $\rho_c \in [0, \rho]$. Here, $\rho_c = \rho$ indicates that all vehicles in the grid are regulatable.
- v : the average longitudinal vehicle velocity within the grid.
- v_c : the average longitudinal velocity of CVs within the grid.

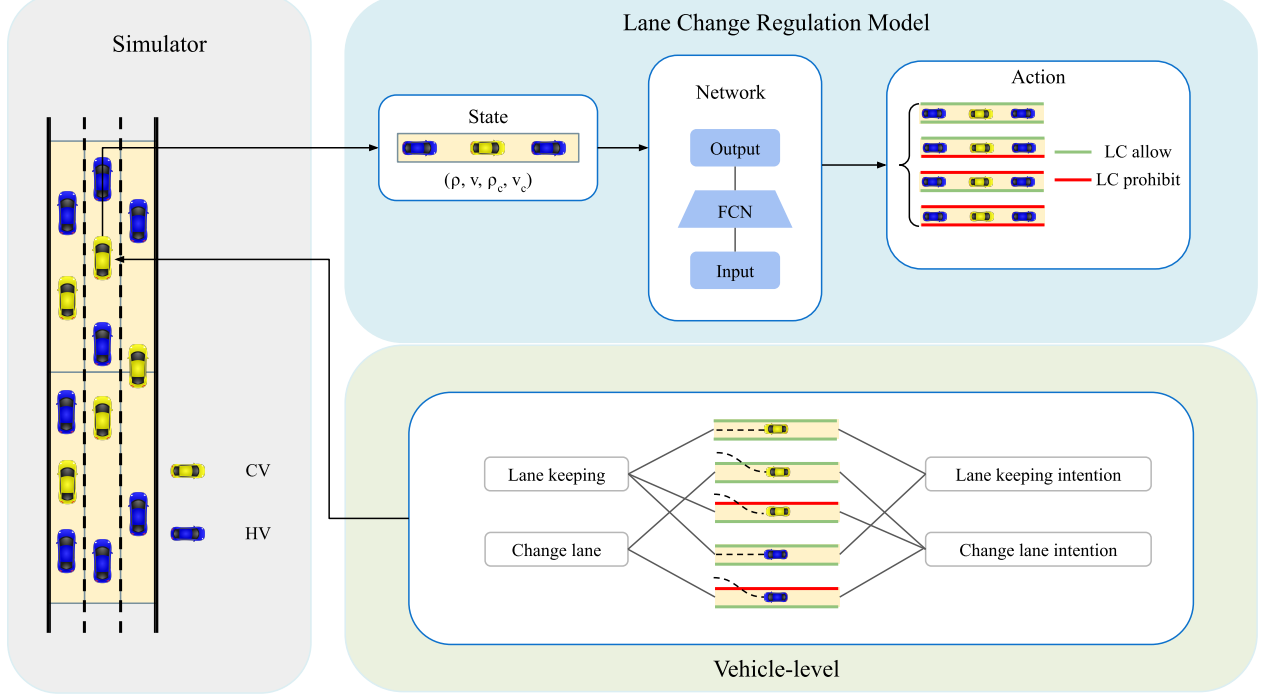


Fig. 2. Hierarchical architecture of the proposed lane-change regulation model, integrating the microscopic traffic simulator SUMO for vehicle-level dynamics and macroscopic traffic PDEs for aggregated lane-change decisions.

In Section II-B, we derive the dynamics model in a fully regulatable environment. This model can be extended to a partially regulatable environment where both HVs and CVs coexist. We assume that HVs and CVs follow the same microscopic models, as CVs are essentially HVs equipped with connectivity functionalities. This assumption of driving behavioral homogeneity ensures that the fundamental diagram and the parameters such as T^{left} and T^{right} in Eq. (5) and (6) depend only on the combined density, velocity, and flow of both CVs and HVs. The evolution of density and velocity for either CV or HV is governed by the same equations, as expressed in Eq. (5) and (6), while regulation actions are applied only to CVs.

The observation space for each grid Ω_{α_i} is a subset of the global state. In our setting, the observation is denoted as $\Omega_{\alpha_i} = \{S_{\mathcal{I}_{\alpha}, \mathcal{N}_i}\}$, where $\mathcal{N}_i \subset \{1, \dots, N_x\}$ and $\mathcal{I}_{\alpha} \subset \{1, \dots, m\}$.

2) *Action space*: As described in Section II-B, the action space \mathcal{A}_{α_i} for the grid α_i is two-dimensional. Only the lane change requests from CVs are regulated by the action output.

$$a_{t, \alpha_i} \sim \pi_{\theta}(\mathbf{o}_{t, \alpha_i}) \quad (17)$$

It is important to note that lane change requests from individual vehicles already meet the safety criterion defined in the microscopic physical models. This facilitates the design of the reward function for the proposed model π_{θ} , as safety measures do not need to be explicitly included.

3) *Reward function*: The reward function evaluates the local performance of each grid agent, focusing primarily on traffic efficiency by assessing congestion levels. A comprehensive review of road traffic congestion measures is provided in [56].

The reward r_1 measures efficiency based on the speed performance index [57]. For a given grid agent α_i with local area $\mathcal{B}(\alpha_i)$, r_1 is defined as:

$$r_1 = \frac{1}{|\mathcal{B}(\alpha_i)|} \sum_{\tilde{\alpha}_k \in \mathcal{B}(\alpha_i)} \frac{v_{\tilde{\alpha}_k}}{v_{max}}, \quad (18)$$

Here, the aggregated speed information of all vehicles in a grid is evaluated, rather than just the regulatable vehicles. This approach is chosen because the objective is to improve overall traffic efficiency through the actions of regulatable CVs.

We also consider traffic density by defining r_2 based on the volume-to-capacity ratio (V/C):

$$r_2 = \frac{1}{|\mathcal{B}(\alpha_i)|} \sum_{\tilde{\alpha}_k \in \mathcal{B}(\alpha_i)} \left(1 - \frac{\rho_{\tilde{\alpha}_k}}{\rho_{max}} \right). \quad (19)$$

Unlike the discretized Level of Service (LOS) indicator used in [56], we adopt a continuous function with respect to ρ as defined in Eq. (19). This choice ensures training stability, especially in scenarios with high-frequency oscillations, whereas the LOS value can fluctuate significantly over time.

In Eq. (18) and (19), v_{max} and ρ_{max} are determined by the simulation settings, as shown in Table III. The overall reward

function for grid agent α_i is defined as a weighted sum of r_1 and r_2 :

$$r = w_1 r_1 + w_2 r_2. \quad (20)$$

The $\mathcal{B}(\alpha_i)$ used in all the experiments includes all grids within a rectangular area:

$$\mathcal{B}(\alpha_i) = \{\tilde{\alpha}_k | \tilde{\alpha} = \alpha - 1, \alpha, \alpha + 1; |x_i - x_k| \leq 2\Delta x\} \quad (21)$$

We train our policy using Double Deep Q-Network (Double DQN) algorithm, which offers significant advantages for traffic flow control tasks. Double DQN addresses overestimation bias commonly encountered in traditional Deep Q-Networks (DQN) by decoupling action selection from value estimation [58]. This improves training stability and provides more accurate value function estimates. The proposed training algorithm is detailed in Algorithm 1.

Algorithm 1 Double DQN with Multiple Agents

Initialize: Q-network Q_θ , target network Q_{θ^-} , and replay buffer \mathcal{D} .

For step=1, ..., M

 Reset the environment state s_0 .

While not done

For each agent

 Select action with exploration probability ϵ

$a_{t,\alpha_i} = \arg \max_a Q_\theta(s_{t,\alpha_i}, a)$

End

 Execute action $a_t = (a_{t,\alpha_i})$ in environment \mathcal{E}

 observe global reward r_t and next state s_{t+1}

 //Collect data

 Store transition in replay buffer \mathcal{D}

$\mathcal{D} \leftarrow \mathcal{D} \cup (s_t, a_t, r_t, s_{t+1})$

 //Train the model

 Sample $B = \{(s_k, a_k, r_k, s_{k+1})\}$ from \mathcal{D}

For each agent

 Calculate agent reward from global reward

$r_{j,\alpha_i} \sim r_j$ from Eq. (20).

 Compute target Q value:

$y_{j,\alpha_i} = r_{j,\alpha_i} + \gamma Q_{\theta^-}(s_{j+1,\alpha_i}, \arg \max_a Q_\theta(s_{j+1,\alpha_i}, a))$

End

 Reshape batch into \tilde{B} with size of $|B| \times \text{num}_{\text{agents}}$.

 Perform gradient descent on loss

$\mathcal{L}(\theta) = \mathbb{E}_{\tilde{B}}[(y_j - Q_\theta(s_j, a_j))^2]$

If step mod $T_{\text{update}} == 0$

 Update target network $Q_{\theta^-} \leftarrow Q_\theta$.

End

 step \leftarrow step+1

End

Log episode metrics.

End

III. EXPERIMENTAL SETUP

A. Simulation Environment and Settings

We build a 5-lane highway road in the SUMO microscopic simulator [59]. The road length is 1000 m and lane width is 3.2 m. The speed limit of each lane is set to 55 mph. Vehicles arrive from the entrance of the road, and the number of vehicles emitted each second follows a binomial distribution. The intelligent driver model (IDM) [60] is selected as the car-following model for all simulated vehicles. The corresponding parameters settings are shown in Table I. Besides, we set lateral resolution to 0.8m and choose the SL2015 model [61] as the lane-changing model. Table II show the traffic demands used in the simulation scenarios.

The relation of inflow and density is decided by the concave fundamental diagram derived from IDM car-following model, as illustrated in Fig. 3.

TABLE I
PARAMETER SETTING FOR IDM MODEL

Symbol	Description	Value
L	Vehicle length	5 m
v_0	Desired speed	24.59 m/s
T	Time gap	1.4 s
s_0	Minimum gap	2.5 m
δ	Acceleration exponent	4
a	Acceleration	0.73 m/s ²
b	Comfortable deceleration	1.67 m/s ²

TABLE II
TRAFFIC DEMAND SETTINGS IN SIMULATION SCENARIOS

	Inflow (veh/(lane*h))	Density (veh/(lane*m))	Velocity (m/s)
Low demand	1100	0.013	22.93
High demand	1495	0.02	20.76
Congested High demand	1410	0.06	6.53

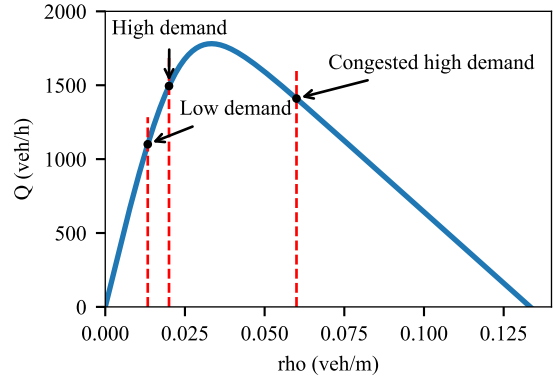


Fig. 3. Demand settings with the fundamental diagram.

Given a demand setting, we test our model in different scenarios. Besides a stable inflow scenarios, typical safety-critical

events are included for evaluating the model performance during unstable transition processes. We name and describe each of the scenarios.

- 1) *Stable Flow*: In a stable flow scenario, all lanes share a constant inflow rate selected from Table II. All vehicles depart from the entry position of the road. The initial state of the system is an empty road, and the system need some time to reach to the stable flow state. The transition time depends on the travel speed of vehicles. All data collected during the transition time is excluded when calculating metrics during both the training and evaluating stages.
- 2) *Lane Degrade*: In a lane degrade scenario, one lane or more, can degrade its capacity due to narrow lane width, dangerous road condition, or reduced visibility range. This can be simulated by assigning increased time gap parameter of IDM model for vehicles in this lane [60]. Built upon a *Stable Flow* scenario, we create lane degrade events with random lane, location range, and time range. The new time gap is set in the range [4.0, 10.0] seconds. Lane change actions are prohibited for all vehicles traveling in hazardous lane grids, regardless of the decisions made by the driver or our model.
- 3) *Vehicle Stop*: In a vehicle stop scenario, a lane block event is created by an accidental vehicle. We simulate this event in this way: at a given trigger time, a vehicle will decelerate relatively aggressively until the speed reaches to zero. Then the vehicle will maintain stopping for a random period of time. During the recovery stage, the accidental vehicle and its blocked followers will resume their route.

B. Training

We train a policy using a Double Deep Q-Network (Double DQN) for each scenario and demand condition, which offers significant advantages for traffic flow control tasks. Double DQN addresses overestimation bias commonly encountered in traditional Deep Q-Networks (DQN) by decoupling action selection from value estimation [58]. This improves training stability and provides more accurate value function estimates.

For each scenario and demand condition, we train a policy using Double DQN. The network employs a fully convolutional neural network (FCN) with ReLU activation functions and a discount factor of 0.95. A training environment is created for each scenario and demand condition using the SUMO simulation framework. Simulation parameters include a unified simulation step $\delta = 0.1s$, a reward step $\Delta t_r = 1.0s$, and an environmental step size $\Delta t_{env} = 4.0s$ for consistency across environments. The reward for each step is the average reward calculated over the interval Δt_{env} , with samples taken at regular intervals of Δt_r . The lane grid length Δx_{env} is set to 100m, as summarized in Table III. After completing an episode, the training environment is reset by regenerating traffic demand with a random seed. If a safety-critical event occurs, parameters such as location range and lane are also randomized.

TABLE III
PRIMARY HYPERPARAMETERS USED DURING TRAINING.

Parameters	Value
lane grid length (m)	100
discount factor γ	0.95
reward weight of speed ω_1	0.5
reward weight of density ω_2	0.5
road max density (veh/(lane*m))	0.133
road max speed (m/s)	24.59

Training is conducted over 250,000 steps, with performance metrics calculated at the end of each episode. Experimental environments including SUMO, Traffic Control Interface (TraCI), and OpenAI Gym APIs are conducted on a computer with a Nvidia GeForce RTX 4090 and 64GB RAM. Python 3.9 was installed with PyTorch 1.13.1.

C. Evaluation

The primary goal of the proposed model is to optimize the efficiency of the entire freeway section. At the same time, we need to monitor whether our model causes negative effect on the driving safety and energy cost. Therefore, traffic efficiency, safety, and energy cost are the performance metrics of interest. In this context, we use average travel speed of all vehicles for evaluating traffic efficiency. The metric of energy cost is CO₂ emission. We adopt *HBEFA3/PC_G_EU4* emission model [62] for all simulated vehicles. Since our model does not intervene directly on vehicle-level maneuvers, collision-free is naturally achieved. Besides the collision rate indicator, time-to-collision (TTC) based measures are also commonly used [33], [63]. When TTC is less than a threshold, a collision risk is indicated. We use two TTC based indicators: average TTC and time exposed TTC (TET) [64]. Compared to average TTC, time exposed TTC is normalized by travel time of each vehicle. The definitions of two safety indicators are given in Eq. (22) and Eq. (23). Critical thresholds TTC* are selected as 5.0s.

$$\overline{\text{TTC}} = \frac{1}{N_{veh}} \sum_{i=1}^{N_{veh}} \sum_{t=1}^{T_i} \mathbf{1}_i(\text{TTC}_i(t) < \text{TTC}^*) \cdot \delta \quad (22)$$

$$\text{TET} = \frac{1}{N_{veh}} \sum_{i=1}^{N_{veh}} \sum_{t=1}^{T_i} \frac{1}{T_i} \cdot \mathbf{1}_i(\text{TTC}_i(t) < \text{TTC}^*) \quad (23)$$

We evaluate models trained in each environment at varying checkpoints. The baseline model is defined to follow the SUMO IDM car-following model and SL2015 lane-changing model for all vehicles. As mentioned in III-A, the average metrics are calculated over 200 episodes, excluding metrics within the transition time.

IV. NUMERICAL RESULTS

This section evaluates the performance of the lane-change regulation model in different traffic scenarios and under different penetration rate of CVs.

A. Performance of the Lane Change Regulation Model

To minimize the dependency on precise parameter initialization and enhance training stability, the states are normalized to the range $[0, 1]$ by dividing each dimension by its respective maximum value. These maximum values of vehicle speed and density are determined by the fundamental diagram. The primary hyperparameters of our algorithm are listed in Table III.

Fig. 4 illustrates the average agent's accumulated reward per episode during the training phase. Under free-flow demand conditions (low and high), a vehicle stop event substantially reduces reward performance. In contrast, compared to congested high demand conditions, a significant improvement trend is observed under free-flow demand conditions across all scenarios. As shown in Fig. 4, this improvement is primarily attributed to the enhancement in the speed performance index reward term associated with vehicle travel speeds. This indicates that the policy seeks to optimize traffic speed without significantly changing the equilibrium state of the traffic, which is governed by the spatial distribution of traffic density.

Table V summarizes the results of our model and the baselines across all evaluation environments. Comparative metrics against the baselines are presented in Table VI, with arrows indicating the optimization direction for each indicator. Our model outperforms the baseline in terms of traffic efficiency under low and high demand conditions, while demonstrating comparable performance under congested high demand conditions. As shown in Table IV, the average number of lane changes per vehicle in the *Stable Flow* scenario decreases by 87% under congested high demand conditions compared to low demand conditions. Moreover, our regulation model significantly suppresses lane-changing behavior compared to the baseline. For example, in the *Stable Flow* scenario, the lane change frequency decreases by 27.8%, 31.3%, and 25.0% under low, high, and congested high demand conditions, respectively. This indicates a link between the optimization strategy of our model and the suppression of lane change frequency. Consequently, it can be inferred that low lane change frequency in congested conditions restricts the optimization potential of our model, leading to its comparable performance under congested high demand conditions.

When energy cost is considered, a clear trade-off emerges between travel efficiency and energy cost in our model's performance. If the trade-off ratio between these two metrics is set to 1:1, our model performs better under high demand conditions compared to low demand conditions. For example, in the *Lane Degrade* scenario under low demand conditions, our model achieves a 2.7% improvement in average speed at the cost of a 2.4% increase in CO_2 emissions. In contrast, under high demand conditions in the same scenario, these values are 3.0% and 1.8%, respectively. Considering the performance uplift margin, it is crucial to assess whether our model consistently achieves these gains. The environment is constructed to ensure fairness in comparison by maintaining the same vehicle route demand, safety-critical event settings, and random seeds in each evaluation rounds for our model and the baseline.

TABLE IV
AVERAGE NUMBER OF LANE CHANGES PER VEHICLE PER EVALUATION EPISODE UNDER VARIOUS DEMAND CONDITIONS.

Scenario	Models	Demand		
		Low	High	Congested High
<i>Stable Flow</i>	Baseline	0.090 \pm 0.011	0.048 \pm 0.011	0.012 \pm 0.012
	Ours	0.065 \pm 0.015	0.033 \pm 0.009	0.009 \pm 0.009
<i>Lane Degrade</i>	Baseline	0.113 \pm 0.023	0.075 \pm 0.023	0.049 \pm 0.030
	Ours	0.077 \pm 0.021	0.051 \pm 0.021	0.043 \pm 0.027
<i>Vehicle Stop</i>	Baseline	0.104 \pm 0.019	0.071 \pm 0.021	0.061 \pm 0.036
	Ours	0.077 \pm 0.019	0.054 \pm 0.020	0.050 \pm 0.032

Fig. 5 shows the distribution of performance uplift across episodes in all environments. In low and high demand conditions, where our model outperforms the baseline, performance uplift is consistent across episodes. The *Stable Flow* scenario exhibits less fluctuation than the *Lane Degrade* and *Vehicle Stop* scenarios, where fluctuations are primarily attributed to safety-critical events. This observation aligns with the higher fluctuation in training rewards under scenarios involving safety-critical events, as shown in Fig. 4.

Regarding safety metrics $\overline{\text{TTC}}$ and TET, our model increases the safety burden by up to 4.2% across different scenarios and demand conditions. However, given the loose threshold of 5.0s and the absence of collision events, the safety performance meets expectations, even though no safety-related term is included in the reward function. This highlights the advantage of our regulation framework in ensuring traffic safety compared to vehicle-level control approaches.

B. Policy Behavior Analysis

Here, we analyze how our model optimizes traffic efficiency through lane-change regulation. The SL2015 lane-change model used in our experiments closely aligns with driver lane-change behaviors in real-world freeways, as described in [61]. Specifically, the real-world regulation "Keep to the Right" is represented in SL2015 by the "Keep Right" lane-change intention, where vehicles are obligated to clear the overtaking lane. Additionally, lane changes based on the "Speed Gain" intention are accurately modeled in SL2015, capturing expected speed gains exceeding an empirical threshold. By default, decisions to speed up by changing to the right lane require more deliberation compared to leftward lane changes. To evaluate the policy behavior, we visualize the distribution of actions taken by our model in the *Stable Flow* scenario under low and high demand conditions. Specifically, we compare the action distribution at training checkpoints 100k and 200k for each evaluation environment. Fig. 6 highlights three key observations:

- 1) The policy does not aggressively prohibit lane changes, maintaining at least one direction of lane change action ("Any") above 80% at all times under both demand conditions.
- 2) Since "left allow" = "any" - "right only" and "right allow" = "any" - "left only", the stable policy at checkpoint 200k under both demand conditions exhibits a

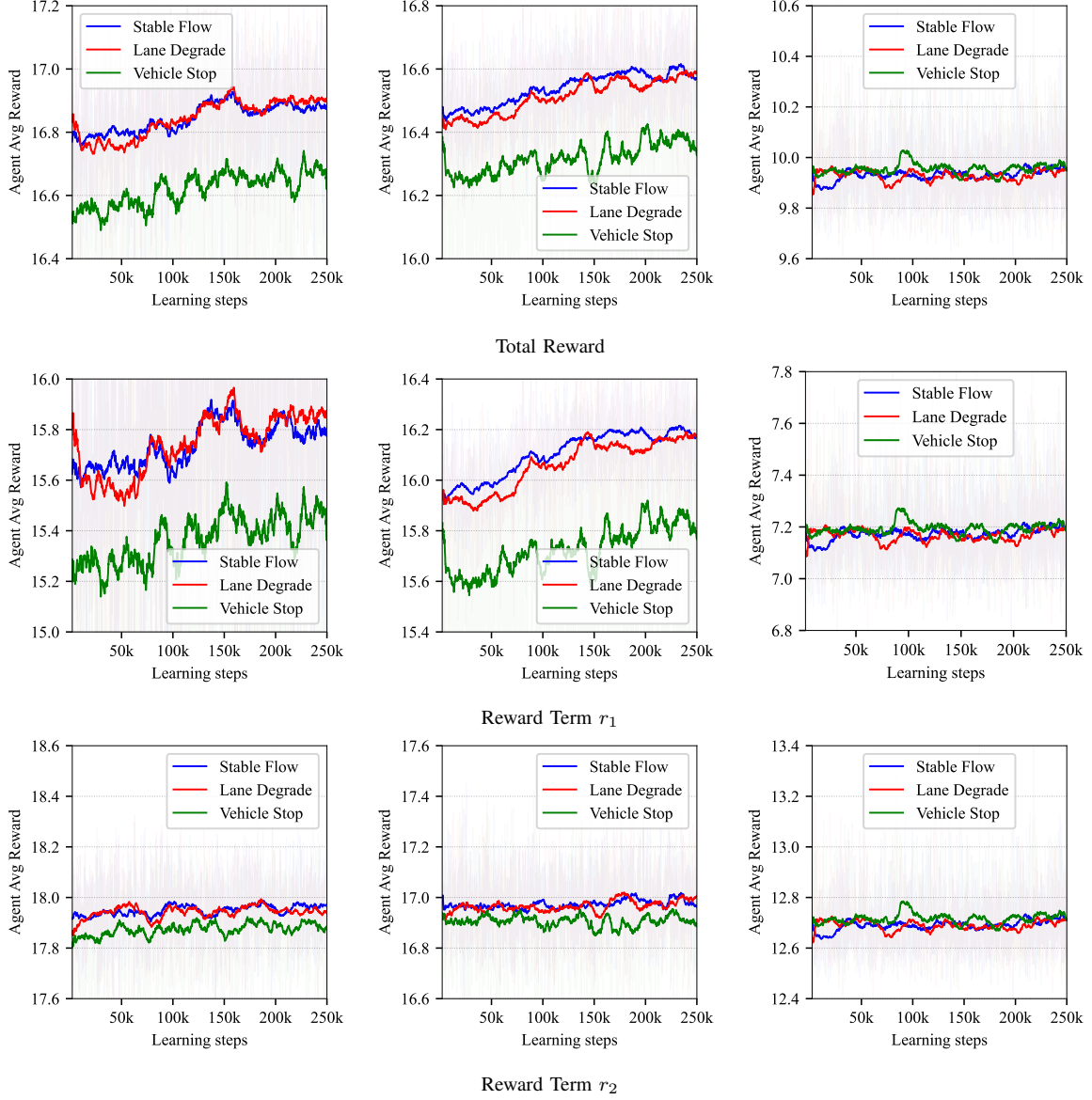


Fig. 4. Average agent reward per episode during the training phase under varying demand environments. From left to right, the columns represent low, high, and congested high demand conditions. The top row shows the total reward, while the second and third rows present the rewards for terms r_1 and r_2 , respectively. The solid lines indicate a moving average with a window size of 60 episodes.

significantly higher "right only" rate compared to "left only." This suggests that the policy suppresses leftward lane changes more than rightward ones, as leftward changes are solely associated with speed gain intentions, which reflect aggressive and egocentric driving behavior.

3) The policy demonstrates heterogeneity across lanes, particularly in its restrictions on leftward lane changes. From the rightmost to the leftmost lane, the model progressively relaxes constraints on left lane change decisions represented by the "left allow" rate.

Through this analysis, we further evaluate the performance of the policy trained in the *Stable Flow* scenario when applied to other scenarios. As shown in Table VII, cross-validation performance deteriorates under high demand conditions while remaining comparable under low demand conditions. For

instance, the uplift in average speed decreases by 33%, from 3.0% to 2.0%, in the *Lane Degrade* scenario under high demand conditions. This performance discrepancy can be attributed to the vehicle density differences between the two demand conditions. The sparse vehicle distribution under low demand conditions mitigates the impact of safety-critical events, whereas out-of-distribution congested traffic states induced by safety-critical events under high demand conditions are the primary cause of poor performance.

C. Performance under Varying Penetration Rate of CVs

In the previous experiments, all vehicles were regulatable (i.e., 100% of vehicles were CVs). Here, we investigate how the performance of our model changes under different CV rates. For a given regulation rate, vehicles are randomly

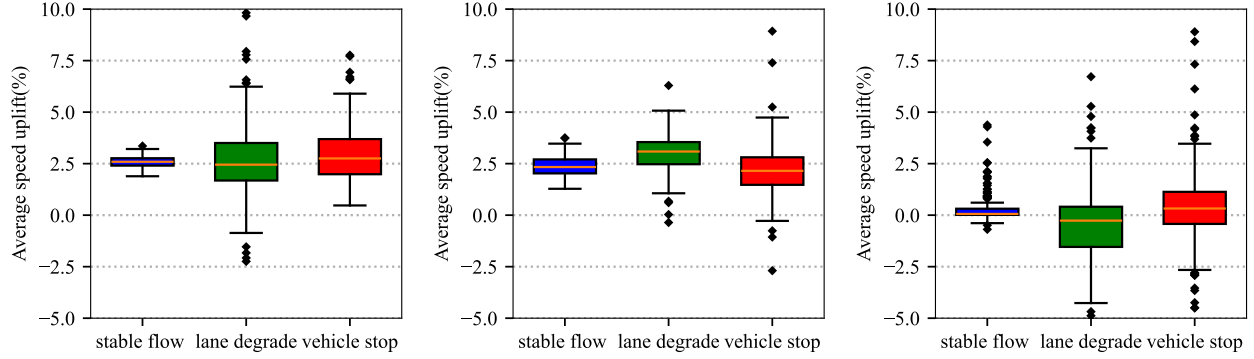


Fig. 5. Boxplots of performance uplift across episodes under varied demand conditions. Each environment is evaluated over 200 episodes. From left to right, the plots represent low, high, and congested high demand conditions. The colored boxes represent the interquartile range (IQR) containing 50% of the data near the median. Outliers are shown as black diamonds.

TABLE V
PERFORMANCE METRICS (MEAN AND STANDARD DEVIATION) ACROSS SCENARIOS UNDER DIFFERENT DEMAND CONDITIONS.

Metric	Demand	Stable Flow		Lane Degrade		Vehicle Stop	
		Baseline	Our model	Baseline	Our model	Baseline	Our model
Average speed(m/s)	Low	21.77 \pm 0.11	22.33 \pm 0.09	20.87 \pm 0.72	21.42 \pm 0.62	20.84 \pm 0.51	21.46 \pm 0.46
	High	19.33 \pm 0.16	19.8 \pm 0.16	18.83 \pm 0.38	19.4 \pm 0.42	18.86 \pm 0.31	19.27 \pm 0.32
	Congested High	8.54 \pm 0.12	8.56 \pm 0.15	8.87 \pm 0.36	8.83 \pm 0.33	8.84 \pm 0.42	8.9 \pm 0.47
CO2 emission(g)	Low	161.21 \pm 0.92	165.86 \pm 0.83	168.0 \pm 7.58	172.11 \pm 7.84	172.35 \pm 9.26	176.83 \pm 9.43
	High	157.53 \pm 1.09	160.25 \pm 1.18	167.07 \pm 9.48	170.13 \pm 9.11	170.84 \pm 8.37	173.43 \pm 8.14
	Congested High	256.5 \pm 3.24	256.25 \pm 3.83	259.56 \pm 11.85	259.93 \pm 11.83	259.24 \pm 7.83	258.87 \pm 8.19
TTC(s)	Low	0.0 \pm 0.0	0.0 \pm 0.0	0.29 \pm 0.27	0.3 \pm 0.28	0.35 \pm 0.19	0.35 \pm 0.18
	High	0.0 \pm 0.0	0.0 \pm 0.0	0.25 \pm 0.2	0.25 \pm 0.21	0.28 \pm 0.12	0.29 \pm 0.12
	Congested High	3.01 \pm 0.28	2.98 \pm 0.29	2.86 \pm 0.46	2.88 \pm 0.46	2.7 \pm 0.58	2.67 \pm 0.62
TET(%)	Low	0.0 \pm 0.0	0.0 \pm 0.0	0.25 \pm 0.21	0.25 \pm 0.21	0.29 \pm 0.18	0.27 \pm 0.15
	High	0.0 \pm 0.0	0.0 \pm 0.0	0.16 \pm 0.11	0.17 \pm 0.12	0.19 \pm 0.11	0.2 \pm 0.11
	Congested High	2.37 \pm 0.23	2.34 \pm 0.23	2.15 \pm 0.29	2.18 \pm 0.28	2.07 \pm 0.46	2.05 \pm 0.49

assigned as CVs in proportion to the specified rate, and the model is trained and evaluated in the corresponding environment. We select two of the best-performing scenarios in terms of traffic efficiency for analysis. Fig. 7 presents the training rewards and evaluation performance under varying penetration rate of CVs.

As the regulation rate decreases from 100% to 50%, the average agent reward per episode during training decreases in both evaluation scenarios. The evaluation results reveal that both average speed and CO₂ emissions decrease significantly. In Section IV-A, we concluded that, considering both efficiency and energy cost, the model performs slightly better than the baseline in the *Stable Flow* scenario under low demand conditions and outperforms the baseline in the *Lane Degrade* scenario under high demand conditions. These conclusions remain valid when the regulation rate is below 100% but above a certain threshold, although the *Lane Degrade* scenario exhibits greater performance variability compared to the *Stable Flow* scenario. These findings suggest that our model maintains consistent performance across a range of regulation rates.

V. CONCLUSION

This paper presents a novel lane change regulation model designed to enhance overall traffic efficiency. The approach introduces the concept of regulating individual connected vehicle lane change decisions through a macroscopic traffic control framework. A multi-agent reinforcement learning algorithm is proposed, wherein the action space determines whether to permit or prohibit lane change actions within each lane grid. Simulation environments are constructed across various scenarios and demand conditions to comprehensively evaluate the performance of the proposed model.

In scenarios where 100% of vehicles are regulatable, experimental results demonstrate that our model achieves comparable or superior performance relative to the baseline when balancing traffic efficiency and energy cost. Performance analysis reveals that the model effectively suppresses leftward lane changes to varying extents across different lanes. Additionally, experiments with varying regulation rates indicate that the model continues to positively influence traffic flow as long as the control rate remains above a certain threshold.

Three promising directions for future research are identified.

TABLE VI
COMPARISON OF PERFORMANCE METRICS BETWEEN THE PROPOSED MODEL AND BASELINES ACROSS SCENARIOS UNDER VARYING DEMAND CONDITIONS.

Metric	Stable Flow			Lane Degrade			Vehicle Stop		
	Low	High	Congested	Low	High	Congested	Low	High	Congested
Average Speed (\uparrow)	2.6	2.4	0.3	2.7	3.0	-0.5	2.7	2.2	0.5
CO2 Emission (\downarrow)	2.9	1.7	-0.1	2.4	1.8	0.1	2.6	1.5	-0.1
TTC (\downarrow)	-*	-	-1.2	4.2	0.7	1.0	-1.4	2.5	-1.2
TET (\downarrow)	-	-	-1.2	-	-	1.2	-	-	-1.2

*The values of both the baseline and the proposed model are close to zero.

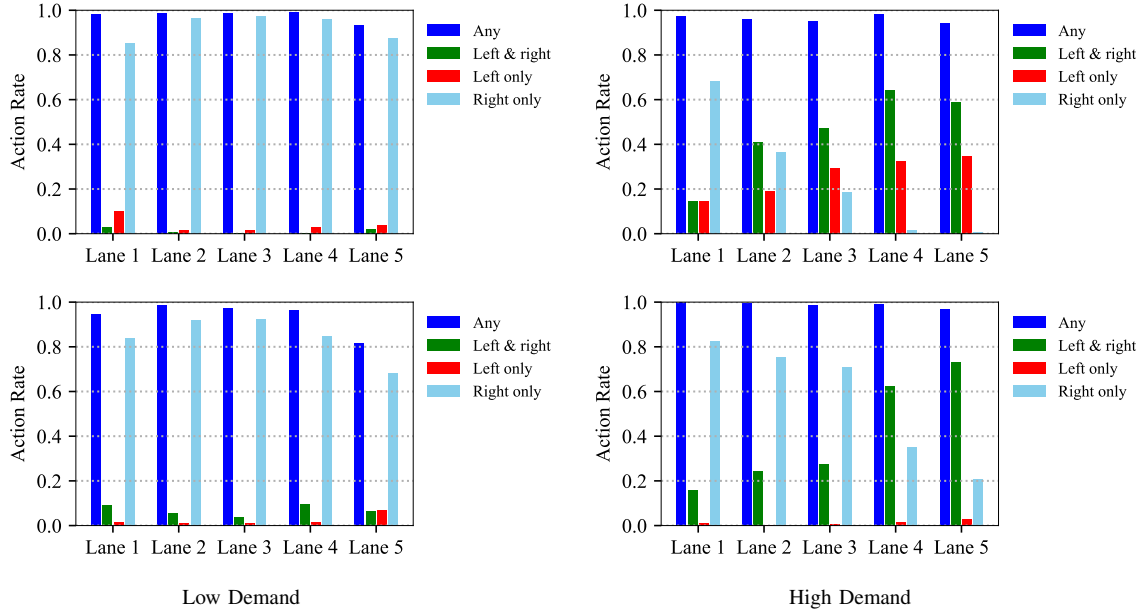


Fig. 6. Distribution of actions across different training checkpoints for the *Stable Flow* scenario under low and high demand conditions. The training steps for each checkpoint, from top to bottom, are 100k and 200k steps. The lane index starts from 1, corresponding to the rightmost lane. Actions are collected every 1000 steps during evaluation for all lane grids along each lane.

TABLE VII
CROSS-EVALUATION RESULTS OF THE MODEL TRAINED IN THE *Stable Flow* SCENARIO APPLIED TO OTHER SCENARIOS.

Metric	Lane Degrade		Vehicle Stop	
	Low	High	Low	High
Average Speed (\uparrow)	2.7/3.1*	3.0/2.0	2.7/2.4	2.2/1.6
CO2 Emission (\downarrow)	2.4/3.3	1.8/1.4	2.6/3.0	1.5/1.3
TTC (\downarrow)	4.2/7.7	0.7/5.0	-1.4/6.9	2.5/2.5

*The value on the left is from Table VI, while the number on the right is from model cross validation.

First, the current model assumes that all connected vehicles fully comply with regulation signals. However, individual objectives may conflict with the global goal, potentially leading to regulation violations. To address this, future work can incorporate a high-fidelity simulator that models human compliance behavior. Since cross-environment experiments reveal performance degradation, exploring methods to train

a unified, generalized policy adaptable to varied demand conditions and scenarios deserves investigation. Finally, real-world deployment requires bridging the simulation-to-reality gap. Future work should focus on faithfully reproducing a wider range of real-world demand conditions and scenarios within the simulator.

REFERENCES

- [1] S. Cui, B. Seibold, R. Stern, and D. B. Work, "Stabilizing traffic flow via a single autonomous vehicle: Possibilities and limitations," in *2017 IEEE Intelligent Vehicles Symposium (IV)*. IEEE, 2017, pp. 1336–1341.
- [2] R. E. Stern, S. Cui, M. L. Delle Monache, R. Bhadani, M. Bunting, M. Churchill, N. Hamilton, H. Pohlmann, F. Wu, B. Piccoli *et al.*, "Dissipation of stop-and-go waves via control of autonomous vehicles: Field experiments," *Transportation Research Part C: Emerging Technologies*, vol. 89, pp. 205–221, 2018.
- [3] A. Talebpour and H. S. Mahmassani, "Influence of connected and autonomous vehicles on traffic flow stability and throughput," *Transportation research part C: emerging technologies*, vol. 71, pp. 143–163, 2016.
- [4] J. Wang, Y. Zheng, K. Li, and Q. Xu, "Deep-lcc: Data-enabled predictive leading cruise control in mixed traffic flow," *IEEE Transactions on Control Systems Technology*, 2023.

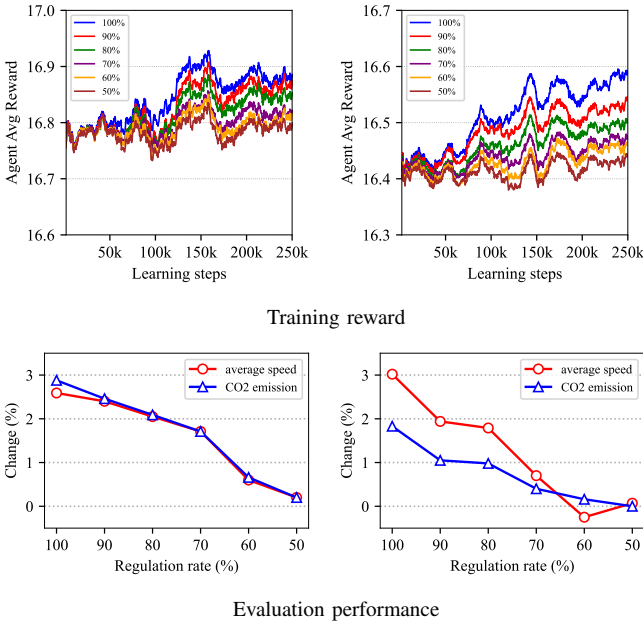


Fig. 7. Training reward per episode and performance metrics under varying regulation rates. Left column: Results for the *Stable Flow* scenario under low demand conditions. Right column: Results for the *Lane Degrade* scenario under high demand conditions.

[5] C. Zhao, H. Yu, and T. G. Molnar, “Safety-critical traffic control by connected automated vehicles,” *Transportation research part C: emerging technologies*, vol. 154, p. 104230, 2023.

[6] C. Zhao, T. G. Molnar, and H. Yu, “Safety-critical stabilization of mixed traffic by pairs of cavs,” in *2024 American Control Conference (ACC)*. IEEE, 2024, pp. 743–748.

[7] Y. Chen, G. Orosz, and T. G. Molnar, “Safety-critical connected cruise control: Leveraging connectivity for safe and efficient longitudinal control of automated vehicles,” in *27th International Conference on Intelligent Transportation Systems*, 2024.

[8] J. Rios-Torres and A. A. Malikopoulos, “Impact of partial penetrations of connected and automated vehicles on fuel consumption and traffic flow,” *IEEE Transactions on Intelligent Vehicles*, vol. 3, no. 4, pp. 453–462, 2018.

[9] I. G. Jin, S. S. Avedisov, C. R. He, W. B. Qin, M. Sadeghpour, and G. Orosz, “Experimental validation of connected automated vehicle design among human-driven vehicles,” *Transportation research part C: emerging technologies*, vol. 91, pp. 335–352, 2018.

[10] A. Vahidi and A. Sciarretta, “Energy saving potentials of connected and automated vehicles,” *Transportation Research Part C: Emerging Technologies*, vol. 95, pp. 822–843, 2018.

[11] M. Čišić, X. Xiong, L. Jin, and K. H. Johansson, “Coordinating vehicle platoons for highway bottleneck decongestion and throughput improvement,” *IEEE Transactions on Intelligent Transportation Systems*, vol. 23, no. 7, pp. 8959–8971, 2021.

[12] V. Milanés, S. E. Shladover, J. Spring, C. Nowakowski, H. Kawazoe, and M. Nakamura, “Cooperative adaptive cruise control in real traffic situations,” *IEEE Transactions on intelligent transportation systems*, vol. 15, no. 1, pp. 296–305, 2013.

[13] N. Hyldmar, Y. He, and A. Prorok, “A fleet of miniature cars for experiments in cooperative driving,” in *2019 International Conference on Robotics and Automation (ICRA)*. IEEE, 2019, pp. 3238–3244.

[14] M. Papageorgiou, H. Hadj-Salem, and F. Middelham, “Alinea local ramp metering: Summary of field results,” *Transportation research record*, vol. 1603, no. 1, pp. 90–98, 1997.

[15] M. Zhang, T. Kim, X. Nie, W. Jin, L. Chu, and W. Recker, “Evaluation of on-ramp control algorithms,” 2001.

[16] E. Smaragdis, M. Papageorgiou, and E. Kosmatopoulos, “A flow-maximizing adaptive local ramp metering strategy,” *Transportation Research Part B: Methodological*, vol. 38, no. 3, pp. 251–270, 2004.

[17] M. Papageorgiou, J.-M. Blosseville, and H. Haj-Salem, “Modelling and real-time control of traffic flow on the southern part of boulevard périphérique in paris: Part ii: Coordinated on-ramp metering,” *Transportation Research Part A: General*, vol. 24, no. 5, pp. 361–370, 1990.

[18] F. Belletti, D. Haziza, G. Gomes, and A. M. Bayen, “Expert level control of ramp metering based on multi-task deep reinforcement learning,” *IEEE Transactions on Intelligent Transportation Systems*, vol. 19, no. 4, pp. 1198–1207, 2017.

[19] H. Yu, S. Park, A. Bayen, S. Moura, and M. Krstic, “Reinforcement learning versus pde backstepping and pi control for congested freeway traffic,” *IEEE Transactions on Control Systems Technology*, vol. 30, no. 4, pp. 1595–1611, 2021.

[20] A. Fares and W. Gomaa, “Freeway ramp-metering control based on reinforcement learning,” in *11th IEEE International Conference on Control & Automation (ICCA)*. IEEE, 2014, pp. 1226–1231.

[21] F. Deng, J. Jin, Y. Shen, and Y. Du, “Advanced self-improving ramp metering algorithm based on multi-agent deep reinforcement learning,” in *2019 IEEE Intelligent Transportation Systems Conference (ITSC)*. IEEE, 2019, pp. 3804–3809.

[22] V. Milanés, J. Godoy, J. Villagrà, and J. Pérez, “Automated on-ramp merging system for congested traffic situations,” *IEEE Transactions on Intelligent Transportation Systems*, vol. 12, no. 2, pp. 500–508, 2010.

[23] T. Chen, M. Wang, S. Gong, Y. Zhou, and B. Ran, “Connected and automated vehicle distributed control for on-ramp merging scenario: A virtual rotation approach,” *Transportation Research Part C: Emerging Technologies*, vol. 133, p. 103451, 2021.

[24] X. Liao, Z. Wang, X. Zhao, K. Han, P. Tiwari, M. J. Barth, and G. Wu, “Cooperative ramp merging design and field implementation: A digital twin approach based on vehicle-to-cloud communication,” *IEEE Transactions on Intelligent Transportation Systems*, vol. 23, no. 5, pp. 4490–4500, 2021.

[25] W. Cao, M. Mukai, T. Kawabe, H. Nishira, and N. Fujiki, “Cooperative vehicle path generation during merging using model predictive control with real-time optimization,” *Control Engineering Practice*, vol. 34, pp. 98–105, 2015.

[26] Y. Zhou, M. E. Cholette, A. Bhaskar, and E. Chung, “Optimal vehicle trajectory planning with control constraints and recursive implementation for automated on-ramp merging,” *IEEE Transactions on Intelligent Transportation Systems*, vol. 20, no. 9, pp. 3409–3420, 2018.

[27] N. Chen, B. van Arem, T. Alkimi, and M. Wang, “A hierarchical model-based optimization control approach for cooperative merging by connected automated vehicles,” *IEEE Transactions on Intelligent Transportation Systems*, vol. 22, no. 12, pp. 7712–7725, 2020.

[28] J. Guo, S. Cheng, and Y. Liu, “Merging and diverging impact on mixed traffic of regular and autonomous vehicles,” *IEEE Transactions on Intelligent Transportation Systems*, vol. 22, no. 3, pp. 1639–1649, 2020.

[29] X. Zhang, L. Wu, H. Liu, Y. Wang, H. Li, and B. Xu, “High-speed ramp merging behavior decision for autonomous vehicles based on multi-agent reinforcement learning,” *IEEE Internet of Things Journal*, 2023.

[30] T. Pan, W. H. Lam, A. Sumalee, and R. Zhong, “Modeling the impacts of mandatory and discretionary lane-changing maneuvers,” *Transportation research part C: emerging technologies*, vol. 68, pp. 403–424, 2016.

[31] R. Xu, L. Huang, S. Yin, D. Yao, H. Zhang, and L. Peng, “An analysis on traffic flow characteristics and lane changing behaviors in beijing urban expressway bottlenecks,” in *2011 14th International IEEE Conference on Intelligent Transportation Systems (ITSC)*. IEEE, 2011, pp. 822–827.

[32] Z. Wang, X. Shi, and X. Li, “Review of lane-changing maneuvers of connected and automated vehicles: models, algorithms and traffic impact analyses,” *Journal of the Indian Institute of Science*, vol. 99, pp. 589–599, 2019.

[33] F. V. Monteiro and P. Ioannou, “Safe autonomous lane changes and impact on traffic flow in a connected vehicle environment,” *Transportation research part C: emerging technologies*, vol. 151, p. 104138, 2023.

[34] M. Menendez and C. F. Daganzo, “Effects of hov lanes on freeway bottlenecks,” *Transportation Research Part B: Methodological*, vol. 41, no. 8, pp. 809–822, 2007.

[35] A. Naseri, F. Estelaji, A. Samani, R. Omidifar, R. Zahedi, and H. Yousefi, “Simulating the performance of hov lanes for optimal urban traffic management,” *Transportation research interdisciplinary perspectives*, vol. 23, p. 101010, 2024.

[36] D. Lin, L. Li, and S. E. Jabari, “Pay to change lanes: A cooperative lane-changing strategy for connected/automated driving,” *Transportation Research Part C: Emerging Technologies*, vol. 105, pp. 550–564, 2019.

[37] M. Tajalli, R. Niroumand, and A. Hajbabaie, “Distributed cooperative trajectory and lane changing optimization of connected automated vehicles: Freeway segments with lane drop,” *Transportation research part C: emerging technologies*, vol. 143, p. 103761, 2022.

[38] H. Xu, Y. Zhang, C. G. Cassandras, L. Li, and S. Feng, "A bi-level cooperative driving strategy allowing lane changes," *Transportation research part C: emerging technologies*, vol. 120, p. 102773, 2020.

[39] S. Bhalla, S. Ganapathi Subramanian, and M. Crowley, "Deep multi agent reinforcement learning for autonomous driving," in *Canadian Conference on Artificial Intelligence*. Springer, 2020, pp. 67–78.

[40] D. Chen, M. R. Hajidavalloo, Z. Li, K. Chen, Y. Wang, L. Jiang, and Y. Wang, "Deep multi-agent reinforcement learning for highway on-ramp merging in mixed traffic," *IEEE Transactions on Intelligent Transportation Systems*, vol. 24, no. 11, pp. 11 623–11 638, 2023.

[41] M. Hua, D. Chen, X. Qi, K. Jiang, Z. E. Liu, Q. Zhou, and H. Xu, "Multi-agent reinforcement learning for connected and automated vehicles control: Recent advancements and future prospects," *arXiv preprint arXiv:2312.11084*, 2023.

[42] C. Vignon, J. Rabault, J. Vasanth, F. Alcántara-Ávila, M. Mortensen, and R. Vinuesa, "Effective control of two-dimensional rayleigh–bénard convection: Invariant multi-agent reinforcement learning is all you need," *Physics of Fluids*, vol. 35, no. 6, 2023.

[43] T. Sonoda, Z. Liu, T. Itoh, and Y. Hasegawa, "Reinforcement learning of control strategies for reducing skin friction drag in a fully developed turbulent channel flow," *Journal of Fluid Mechanics*, vol. 960, p. A30, 2023.

[44] L. Guastoni, J. Rabault, P. Schlatter, H. Azizpour, and R. Vinuesa, "Deep reinforcement learning for turbulent drag reduction in channel flows," *The European Physical Journal E*, vol. 46, no. 4, p. 27, 2023.

[45] S. Peitz, J. Stenner, V. Chidananda, O. Wallscheid, S. L. Brunton, and K. Taira, "Distributed control of partial differential equations using convolutional reinforcement learning," *Physica D: Nonlinear Phenomena*, vol. 461, p. 134096, 2024.

[46] M. Treiber and A. Kesting, "Traffic flow dynamics," *Traffic Flow Dynamics: Data, Models and Simulation*, Springer-Verlag Berlin Heidelberg, pp. 983–1000, 2013.

[47] A. Aw and M. Rascle, "Resurrection of" second order" models of traffic flow," *SIAM journal on applied mathematics*, vol. 60, no. 3, pp. 916–938, 2000.

[48] H. M. Zhang, "A non-equilibrium traffic model devoid of gas-like behavior," *Transportation Research Part B: Methodological*, vol. 36, no. 3, pp. 275–290, 2002.

[49] V. Shvetsov and D. Helbing, "Macroscopic dynamics of multilane traffic," *Physical review E*, vol. 59, no. 6, p. 6328, 1999.

[50] K. N. Porfyri, A. I. Delis, I. K. Nikolos, and M. Papageorgiou, "Calibration and validation of a macroscopic multi-lane traffic flow model using a differential evolution algorithm," in *Transportation Research Board 96th Annual Meeting*. Washington DC, USA: TRB, 2017, pp. 1–17.

[51] J. Song and S. Karni, "A second order traffic flow model with lane changing," *Journal of Scientific Computing*, vol. 81, no. 3, pp. 1429–1445, 2019.

[52] H. Yu and M. Krstic, "Output feedback control of two-lane traffic congestion," *Automatica*, vol. 125, p. 109379, 2021.

[53] H. Holden and N. H. Risebro, "The continuum limit of follow-the-leader models-a short proof," *arXiv preprint arXiv:1709.07661*, 2017.

[54] A. Aw, A. Klar, M. Rascle, and T. Materne, "Derivation of continuum traffic flow models from microscopic follow-the-leader models," *SIAM Journal on applied mathematics*, vol. 63, no. 1, pp. 259–278, 2002.

[55] S. Fan and B. Seibold, "Data-fitted first-order traffic models and their second-order generalizations: Comparison by trajectory and sensor data," *Transportation research record*, vol. 2391, no. 1, pp. 32–43, 2013.

[56] T. Afrin and N. Yodo, "A survey of road traffic congestion measures towards a sustainable and resilient transportation system," *Sustainability*, vol. 12, no. 11, p. 4660, 2020.

[57] F. He, X. Yan, Y. Liu, and L. Ma, "A traffic congestion assessment method for urban road networks based on speed performance index," *Procedia engineering*, vol. 137, pp. 425–433, 2016.

[58] H. Van Hasselt, A. Guez, and D. Silver, "Deep reinforcement learning with double q-learning," in *Proceedings of the AAAI conference on artificial intelligence*, vol. 30, no. 1, 2016.

[59] P. A. Lopez, M. Behrisch, L. Bieker-Walz, J. Erdmann, Y.-P. Flötteröd, R. Hilbrich, L. Lücken, J. Rummel, P. Wagner, and E. Wießner, "Microscopic traffic simulation using sumo," in *2018 21st international conference on intelligent transportation systems (ITSC)*. IEEE, 2018, pp. 2575–2582.

[60] M. Treiber, A. Hennecke, and D. Helbing, "Congested traffic states in empirical observations and microscopic simulations," *Physical review E*, vol. 62, no. 2, p. 1805, 2000.

[61] J. Erdmann, "Sumo's lane-changing model," in *Modeling Mobility with Open Data: 2nd SUMO Conference 2014 Berlin, Germany, May 15–16, 2014*. Springer, 2015, pp. 105–123.

[62] D. Krajzewicz, M. Behrisch, P. Wagner, R. Luz, and M. Krümmow, "Second generation of pollutant emission models for sumo," in *Modeling Mobility with Open Data: 2nd SUMO Conference 2014 Berlin, Germany, May 15–16, 2014*. Springer, 2015, pp. 203–221.

[63] H. Behbahani, N. Nadimi, and S. Naseralavi, "New time-based surrogate safety measure to assess crash risk in car-following scenarios," *Transportation Letters*, vol. 7, no. 4, pp. 229–238, 2015.

[64] M. M. Minderhoud and P. H. Bovy, "Extended time-to-collision measures for road traffic safety assessment," *Accident Analysis & Prevention*, vol. 33, no. 1, pp. 89–97, 2001.